



HAL
open science

Quasi-additivity of the radiative effects of marine cloud brightening and stratospheric sulfate aerosol injection

Olivier Boucher, Christoph Kleinschmitt, Gunnar Myhre

► To cite this version:

Olivier Boucher, Christoph Kleinschmitt, Gunnar Myhre. Quasi-additivity of the radiative effects of marine cloud brightening and stratospheric sulfate aerosol injection. *Geophysical Research Letters*, 2017, 44, pp.11,158-11,165. 10.1002/2017GL074647 . insu-03727046

HAL Id: insu-03727046

<https://insu.hal.science/insu-03727046>

Submitted on 27 Jul 2022

HAL is a multi-disciplinary open access archive for the deposit and dissemination of scientific research documents, whether they are published or not. The documents may come from teaching and research institutions in France or abroad, or from public or private research centers.

L'archive ouverte pluridisciplinaire **HAL**, est destinée au dépôt et à la diffusion de documents scientifiques de niveau recherche, publiés ou non, émanant des établissements d'enseignement et de recherche français ou étrangers, des laboratoires publics ou privés.

Copyright

RESEARCH LETTER

10.1002/2017GL074647

Key Points:

- The instantaneous and effective radiative forcings induced by stratospheric sulfate injection differ substantially due to rapid adjustments
- Stratospheric sulfate aerosol injection leads to a significant increase in stratospheric water vapor and decrease in high-level clouds
- The radiative effects of marine cloud brightening and stratospheric sulfate injection nearly add up and have complementary patterns

Supporting Information:

- Supporting Information S1

Correspondence to:

O. Boucher,
olivier.boucher@ipsl.fr

Citation:

Boucher, O., Kleinschmitt, C., & Myhre, G. (2017). Quasi-additivity of the radiative effects of marine cloud brightening and stratospheric sulfate aerosol injection. *Geophysical Research Letters*, *44*, 11, 158–11, 165. <https://doi.org/10.1002/2017GL074647>

Received 20 JUN 2017

Accepted 28 SEP 2017

Accepted article online 6 OCT 2017

Published online 5 NOV 2017

Quasi-Additivity of the Radiative Effects of Marine Cloud Brightening and Stratospheric Sulfate Aerosol Injection

Olivier Boucher¹ , Christoph Kleinschmitt^{2,3} , and Gunnar Myhre⁴ 

¹Institut Pierre-Simon Laplace, Université P. et M. Curie / CNRS, Paris, France, ²Institute of Environmental Physics, Heidelberg University, Heidelberg, Germany, ³Laboratoire de Météorologie Dynamique, Université P. et M. Curie / CNRS, Paris, France, ⁴Center for International Climate and Environmental Research Oslo, Oslo, Norway

Abstract Stratospheric sulfate aerosol injection (SAI) and marine cloud brightening (MCB) are the two most studied solar radiation management techniques. For the first time we combine them in a climate model to investigate their complementarity in terms of both instantaneous and effective radiative forcings. The effective radiative forcing induced by SAI is significantly stronger than its instantaneous counterpart evaluated at the top of atmosphere. Radiative kernel calculations indicate that this occurs because of a significant stratospheric warming and despite a large increase in stratospheric water vapor that strengthens the greenhouse effect. There is also a large decrease in high-level cloudiness induced by a stratification of the upper tropopause. Our model experiments also show that the radiative effects of SAI and MCB are quasi-additive and have fairly complementary patterns in the Tropics. This results in less spatial and temporal variability in the radiative forcing for combined SAI and MCB as compared to MCB alone.

1. Introduction

Solar radiation management (SRM) refers to a range of different techniques which have been proposed to counteract the anthropogenic greenhouse effect by increasing the amount of solar radiation reflected back to space (Boucher et al., 2014; Keith, 2000; Vaughan & Lenton, 2011). Among such techniques, stratospheric aerosol injection (SAI) and marine cloud brightening (MCB) have received the most attention from a climate modeling viewpoint. The concept of SAI dates back from the 1960s (Environmental Pollution Panel, 1965) and has received renewed attention after the Crutzen (2006) publication calling for more research into the subject. The concept of MCB can be traced back to the early realization that the Earth's radiation budget is sensitive to a fairly small variation in the droplet size of low-level clouds and was first proposed as such by Latham (1990) and Salter et al. (2008) with further climate modeling work thereafter (e.g., Alterskjær et al., 2013). Notwithstanding the importance of their associated ethical, legal, technological, and financial issues, it has been shown that both SAI and MCB can exert a negative radiative forcing of several W m^{-2} and therefore have the potential to cool the planet and compensate for at least a fraction of the radiative forcing by anthropogenic greenhouse gases (Boucher et al., 2013). It is also well known that the climate responses of SRM and anthropogenic greenhouse gases do not compensate each other, especially in terms of precipitation and atmospheric circulation changes (Kravitz et al., 2013; Schmidt et al., 2012). The radiative perturbations induced by the two techniques and their associated climate responses are also known to differ to each other as shown by Jones et al. (2011). This is because the two forcing mechanisms lead to radiative forcings with different spatial patterns and different impacts on the atmospheric vertical structure.

The differences in climate response can be analyzed within the framework of radiative forcings, rapid adjustments, and slow climate feedbacks (Sherwood et al., 2015). In this framework one can rigorously distinguish between the (instantaneous) radiative forcing and the effective radiative forcing. Instantaneous radiative forcing (IRF) is traditionally computed from double radiative calls at each time step of a model simulation (i.e., with fixed surface and atmospheric conditions). Effective radiative forcing (ERF) is computed as the difference in radiative fluxes between two parallel simulations (one perturbed and one control simulation) with identical prescribed sea surface temperatures (SST). The differences between instantaneous and effective radiative forcings are attributable to rapid adjustments in atmospheric temperature, humidity, and cloudiness.

Small changes to the land surface may also contribute to rapid adjustments since only the SST are fixed. Overall, the ERF has been shown to be a better predictor of global mean surface temperature change than IRF (Sherwood et al., 2015). It is therefore important to quantify and understand rapid adjustments associated with a particular forcing mechanism.

In this study we discuss the differences between instantaneous radiative forcing and effective radiative forcing for SAI and MCB alone and for their combination. In particular we examine whether the radiative effects of SAI and MCB are additive for a combined forcing typical of what would be required to offset a doubling of the CO₂ atmospheric concentration. Section 2 describes the model and methods used, while results are discussed in section 3.

2. Model and Methods

We use a high-top version of the Laboratoire de Météorologie Dynamique atmospheric general circulation model (Hourdin et al., 2006 version LMDZ5B). The model resolution is 96 points in longitude, 95 points in latitude, and 79 vertical layers. The version with 39 layers has been successfully used in Coupled Model Intercomparison Project phase 5 (CMIP5) (Dufresne et al., 2013), while the version with 79 layers is used in Kleinschmitt et al. (2017) and will serve for CMIP6.

The model now includes a fully interactive stratospheric sulfate sectional aerosol (S3A) model which is fully described in Kleinschmitt et al. (2017). The S3A model is used here to simulate a continuous injection of 10 Tg S yr⁻¹. The sulfur is injected as SO₂ at a height of 17 km at the equator. It is then oxidized into gas phase H₂SO₄ which nucleates and condenses in sulfuric acid-water particles. All relevant microphysical processes (nucleation, condensation, evaporation, coagulation, and sedimentation) are included, which results in a (generally monomodal) size distribution that varies in space and time. It should be noted that aerosols are fully interactive with the radiative scheme; that is, aerosols modify heating rates both in the shortwave (SW) and longwave (LW) parts of the electromagnetic spectrum. The model was shown to perform well against observations for background (i.e., nonvolcanic) conditions and during the aftermath of the Pinatubo eruption (Kleinschmitt et al., 2017). Sedimenting aerosols from the stratosphere do not impact the microphysical properties of ice clouds. High-level cloudiness is derived from an assumed subgrid-scale distribution of water vapor.

For liquid clouds, droplet number concentration is a function of the soluble accumulation mode aerosol mass concentration using a logarithmic dependence (Boucher & Lohmann, 1995):

$$\text{CDNC} = 10^{2.06+0.48 \log_{10} \sum_i m_i} \quad (1)$$

where cloud droplet number concentration (CDNC) is expressed in cm⁻³, m_i is the mass concentration of aerosol species i in $\mu\text{g m}^{-3}$, and the index i runs on accumulation mode soluble species in the model (sulfate, black carbon, organics, and sea salt). Cloud droplet size is then computed from cloud liquid water content and cloud droplet number concentration. We only consider here the cloud albedo effect and ignore any secondary effects related to the impact of cloud droplet size on cloud liquid water path and precipitation, which are highly uncertain and likely to be small (Malavelle et al., 2017). While the parametrization is very simple, the model simulates an IRF due to aerosol-cloud interactions of about -0.8 W m^{-2} between preindustrial and present-day conditions but with little additional contribution from rapid adjustments, a value which is somewhat larger to the Intergovernmental Panel on Climate Change best estimate for ERF of -0.45 W m^{-2} (Boucher et al., 2013). To simulate the effect of MCB, we prescribe an additional concentration accumulation mode sea salt over the ocean between 30°S and 30°N on top of the aerosol climatology. The additional sea salt aerosol is decreased exponentially with height between the ocean surface with a concentration of $10 \mu\text{g m}^{-3}$ and an altitude of 1.5 km with a scale height of 0.5 km. In a first set of experiments we ignore the radiative effects of the additional sea salt aerosol in clear sky. This represents an idealized case for which the sea water is only sprayed in the presence of clouds and has minimal effects in clear sky. However, the clear-sky radiative effect of sea salt was found to be important in some studies (e.g., Niemeier et al., 2013) so we also repeated the experiments with these effects activated in the model.

The model is run with fixed sea surface temperatures (fixed SST) and fixed sea ice cover for present-day conditions. Each experiment is integrated for 10 years. We can thus estimate radiative forcings and rapid adjustments but not the full climate response to the imposed forcings. The land surface temperature can

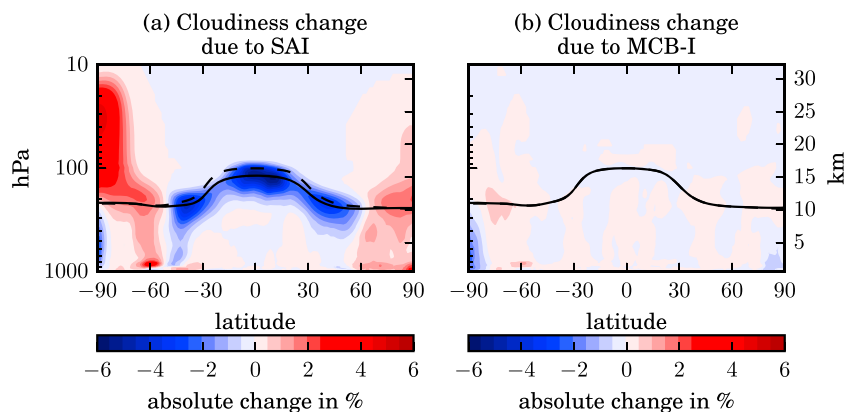


Figure 1. Zonal mean of the absolute change in cloudiness (%) between (a) the SAI and the CONTROL experiments and (b) the MCB-I and the CONTROL experiments. The mean tropopause levels as diagnosed in the SRM and CONTROL experiments are indicated by a solid line and a dashed line, respectively. See also Figures S1 and S4 for the results on additivity.

adjust but only to a limited extent. In conclusion we perform six experiments: a CONTROL experiment with background stratospheric aerosols and accumulation mode aerosols to estimate cloud droplet number concentrations, an SAI experiment which is the same as CONTROL but with a continuous equatorial injection of 10 Tg S yr^{-1} emitted as SO_2 at 17 km altitude, an MCB-I experiment which is the same as CONTROL but with an additional prescribed accumulation mode sea salt aerosol as described above (cloud albedo effect only), an MCB-DI experiment which is the same as MCB-I except that the clear-sky radiative effects of the additional sea salt are also considered, and finally, two experiments (SAI + MCB-I and SAI + MCB-DI) where the perturbations of both the SAI and MCB-I or MCB-DI experiments are combined together. Examination of time series of relevant quantities shows that the model has reached equilibrium after about 3 years. We present hereafter model averages for years 4 to 10. The results of the MCB-DI and SAI + MCB-DI experiments are only shown in the supporting information as they do not change the conclusions.

3. Results

3.1. Rapid Adjustments

The SAI experiment shows a decrease in cirrus cloud, which in annual mean is maximum in the Tropics but extends to midlatitudes (Figure 1a). The maximum actually shifts between hemispheres with the insolation, that is, it occurs in the Northern Hemisphere during June-July-August and in the Southern Hemisphere during December-January-February. The decrease in cirrus is accompanied by a significant lowering of the tropopause in the Tropics.

A decrease in cirrus clouds was already observed in SAI experiments by Kuebbeler et al. (2012), which they attributed to both the role of sulfate aerosols in nucleating cirrus clouds and the stratification of the upper troposphere. As the former mechanism is not included in our model, it is clear that the large rapid adjustments on clouds that we observe are due to thermodynamic and dynamical processes and their impact on cirrus clouds. This said, we cannot be absolutely sure that these rapid adjustments are not an artifact of the model rather than a true feature as the tropopause is a delicate region for climate models to simulate. On one side, the ozone vertical profile is prescribed in our model (i.e., it does not vary with aerosol loading, temperature, and/or circulation changes), which is a limitation of our experimental setup, as the scattering by the aerosol increases significantly ozone absorption in the visible. On the other side, the consistency with the study by Kuebbeler et al. (2012) and the relatively high vertical resolution of our atmospheric model (in comparison to previous simulations) lend more credibility to the results.

The other rapid adjustment in the SAI experiment materializes with an increase in the stratospheric concentration of water vapor (Figure 2a). It is a consequence of a temperature increase of the cold tropopause point which at first order controls the humidity of air masses entering the stratosphere (Figure 3a). An increase in stratospheric water vapor leads to a positive contribution to the ERF. There is a much smaller increase in humidity in the lower stratosphere of the South Pole, which we will come back on later.

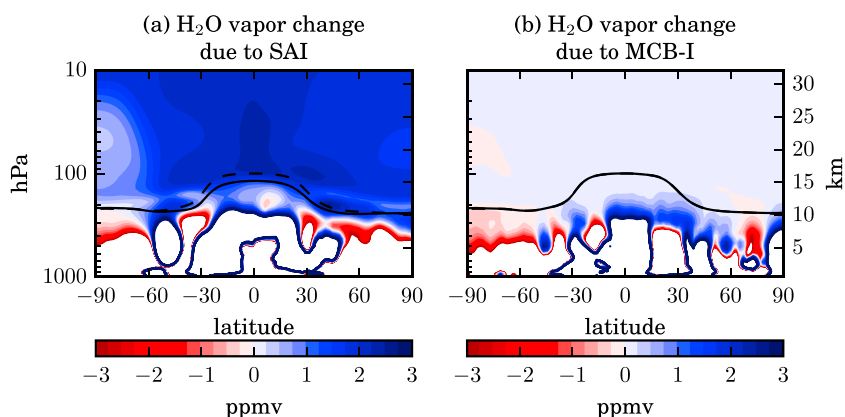


Figure 2. Same as Figure 1 but for the absolute change in stratospheric water vapor (ppmv). White areas correspond to tropospheric changes that are larger than spanned by the color scale. See also Figures S2 and S5 for the results on additivity.

The humidity change can be paralleled to the increase in stratospheric water vapor expected from the climate response to increased greenhouse gases and from methane oxidation in the stratosphere. However, the magnitude of the increase in response to SAI (up to 3 ppm) is larger than the ~ 1 ppm increase associated with global warming (Dessler et al., 2013, 2016; Gettelman et al., 2010) and the ~ 1 ppm from oxidation of methane (Revell et al., 2016) in the 21st climate projections. Furthermore, we do not expect these effects to be necessarily additive in a geoengineered world because the warming of the troposphere due to greenhouse gases would be suppressed by SAI.

Figure 1a also shows increased cloudiness in the polar stratosphere of the Northern and Southern Hemispheres. This increase occurs primarily during winter and spring and is larger in the polar stratosphere of the South Pole. This result may sound surprising; however, it is plausible. The water is condensed by the large-scale condensation scheme of the model, which is triggered by the additional water vapor that enters the tropical lower stratosphere and is transported to the Poles. Stratospheric ice water clouds are not uncommon and have been observed, for example, by Dessler (2009) with the CALIPSO spaceborne lidar. We note that these stratospheric ice clouds tend to dehydrate the stratosphere locally or at least limit the humidity increased due to SAI (see Figure 2a).

We note that rapid adjustments in the SAI experiment also lead to a small global mean surface cooling of 0.15 K and a small global mean precipitation decrease of 8 mm yr⁻¹, which itself is probably induced by more atmospheric absorption. We have performed radiative kernel calculations to quantify the relative importance, in radiative terms, of the rapid adjustments associated to the SAI forcing (Myhre et al., 2011). The largest

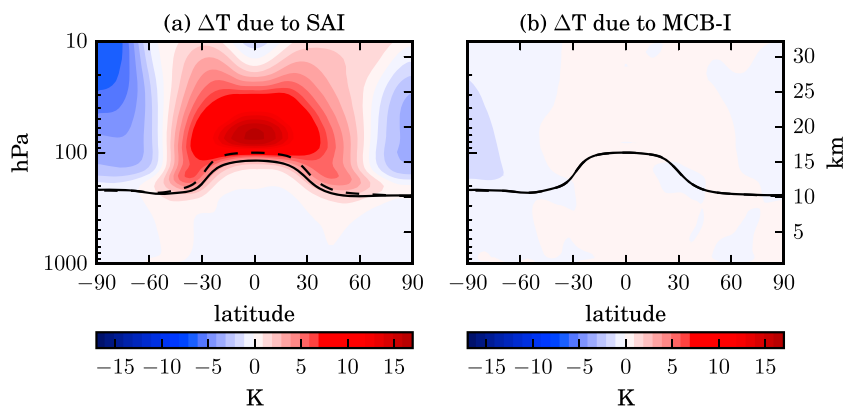


Figure 3. Same as Figure 1 but for the absolute change in temperature (K). See also Figures S3 and S6 for the results on additivity.

Table 1

Decomposition of the Effective Radiative Forcing (ERF) Into Instantaneous Radiative Forcing (IRF) and Radiative Effects Associated With Rapid Adjustments Using the Radiative Kernel Method for the SAI Experiment

	SW	LW	Net
Instantaneous radiative forcing	−4.50	+3.08	−1.43
Change in surface temperature	0.0 ^a	+0.13	+0.13
Change in atmospheric temperature	0.0 ^a	−1.56	−1.56
Change in atmospheric humidity	+0.02	+0.17	+0.19
Residual change (cloud)	+0.94	−0.91	+0.04
Effective radiative forcing	−3.54	+0.91	−2.63

Note. The atmospheric temperature change comprises both the tropospheric and stratospheric temperature changes (but the radiative effects are essentially due to the stratospheric changes). The surface temperature change comprises only land surface as SST are fixed in the experiments. The residual change is computed as the difference between the ERF and the sum of the IRF and other estimated radiative effects. It can be attributed mostly to cloud changes but also has a contribution from surface albedo changes. ^aThese terms are 0 by construction.

contribution from rapid adjustments to the negative ERF comes from the large stratospheric warming (-1.40 W m^{-2} out of a total of -1.56 W m^{-2} due to the overall atmospheric temperature change). It is only partially compensated by the enhanced greenhouse effect due to increased stratospheric humidity (Table 1). The radiative effects induced by cloud changes, diagnosed as the residual from the other terms, appear to be weak, despite a significant decrease in high-level cloudiness. This is due to a near-compensation between the SW (negative) and LW (positive) radiative effects, which is typical for this cloud type in our model.

Rapid adjustments in the MCB simulation are much weaker (Figures 1b, 2b, and 3b). Cloud adjustments in MCB are very small, but the pattern is consistent with a weakening of the Hadley cells, as expected from a cooling of the tropical region (despite the fixed SST conditions). Figure 1b shows decreased cloudiness in the subtropics and a succession of increased and decreased bands of cloudiness when going toward the Poles. Assuming that cloud changes make up the difference between IRF and ERF, we may infer net radiative effects of the order of 0.2 to 0.3 W m^{-2} .

3.2. Spatial Differences Between IRF and ERF

Rapid adjustments in the SAI experiment tend to strengthen the geographical contrasts in IRF as seen on the map of ERF (Figures 4a and 4b and S7a and S7b). The regions of negative IRF show even more negative ERF values, while regions of weakly negative or slightly positive IRF show positive ERF values. The latter is the case in particular over the eastern boundaries of the oceanic basins as well as over Antarctica. The same is true for the MCB experiment with a number of regions (continents and part of the Southern Ocean) with zero IRF (by construction) but a positive ERF (Figures 4c and 4d and S7c and S7d). However, the contrasting regional adjustments in cloudiness result in a rather small radiative effect on the global scale (Table 2).

3.3. Additivity and Complementarity Between SAI and Tropical MCB

The global mean IRF and ERF are remarkably additive for the SAI and MCB experiments (Table 2). While radiative forcing is known not to scale linearly with scattering optical depth (e.g., Boucher et al., 1998), the radiative perturbations in the SAI experiment are too small to be influenced by the presence of MCB (or vice versa). At the grid box level and averaged over years 4 to 10, the IRF of SAI + MCB and the sum of the SAI and MCB IRFs are highly correlated in the 30°S to 30°N region with a correlation coefficient of 0.992 (Figure S8a). The two quantities deviate very little from the 1:1 line, with the IRF of SAI + MCB being slightly smaller (in magnitude) than the sum of the individual IRFs. The ERF of SAI + MCB and the sum of the SAI and MCB ERFs are also highly correlated with a correlation coefficient of 0.89 (Figure S8b).

Figures 4a–4d show how the forcing patterns of our SAI and MCB-I experiments are complementary on an annual mean basis for both IRF and ERF. Over the ocean the regions of large MCB-I forcings correspond to regions of low IRF due to SAI. This is expected because of the larger albedo of the atmosphere underneath the stratospheric (scattering) aerosol layer. What is more surprising is that the complementarity is much stronger

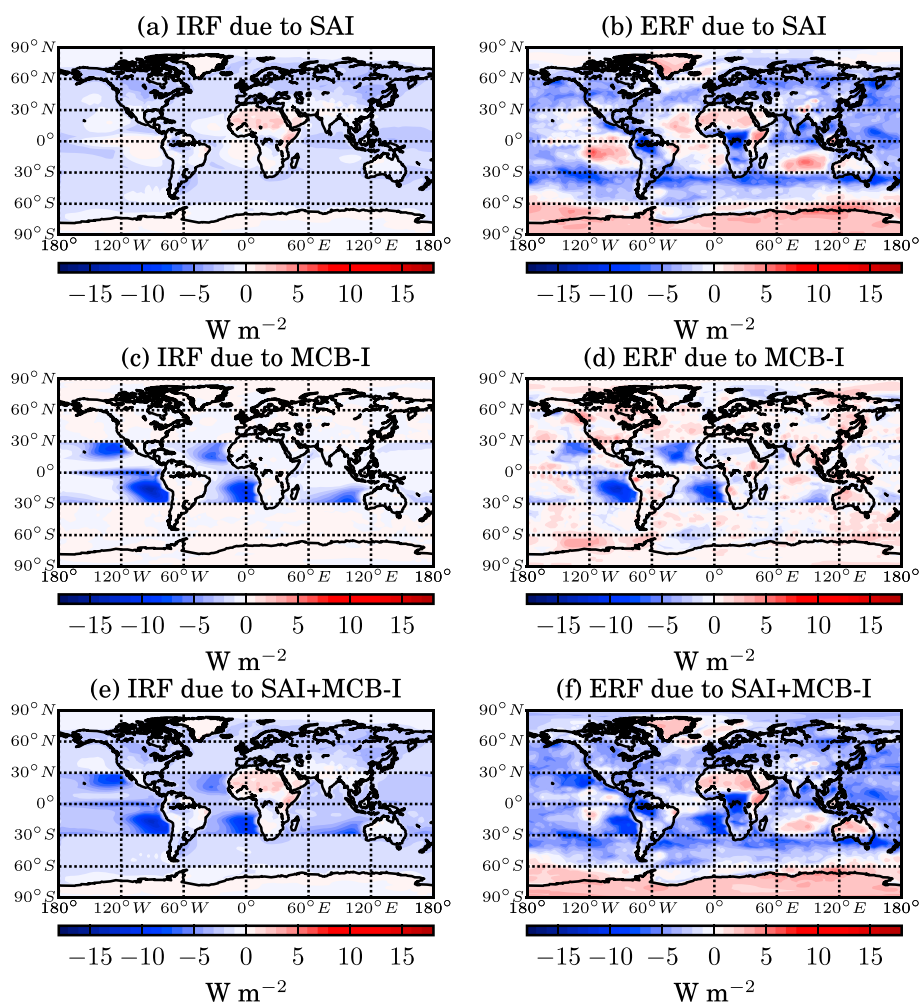


Figure 4. Instantaneous top-of-atmosphere net radiative forcing (IRF, in $W m^{-2}$, Figures 4a, 4c, and 4e) computed from a double radiation call for (a) SAI, (c) MCB-I, and (e) SAI + MCB-I and effective net radiative forcing (ERF, in $W m^{-2}$, Figures 4b, 4d, and 4f) computed from differences in top-of-atmosphere radiative fluxes between parallel fixed-SST experiments for (b) SAI, (d) MCB-I, and (f) SAI + MCB-I. See also Figure S7 for the results with the MCB-DI experiment.

Table 2

Global Mean Quantities and Their Standard Deviations From the SRM Experiments Computed Over the Years 4 to 10 of the Simulations: Top-of-Atmosphere Instantaneous Radiative Forcing (IRF) and Effective Radiative Forcing (ERF) in $W m^{-2}$, Surface Temperature (\bar{T}_s) Change in K, and Precipitation (\bar{P}) Change in $mm yr^{-1}$

		SAI	MCB-I	SAI + MCB-I	Sum SAI and MCB-I ^a
IRF ($W m^{-2}$)	SW	-4.5 ± 0.04	-1.0 ± 0.02	-5.3 ± 0.05	-5.5 ± 0.05
	LW ^b	$+3.1 \pm 0.03$	$+0.0 \pm 0.00$	$+3.1 \pm 0.06$	$+3.1 \pm 0.03$
	net	-1.4 ± 0.02	-1.0 ± 0.02	-2.3 ± 0.02	-2.4 ± 0.03
ERF ($W m^{-2}$)	SW	-3.5 ± 0.24	-0.8 ± 0.21	-4.2 ± 0.15	-4.3 ± 0.32
	LW	$+0.9 \pm 0.12$	$+0.0 \pm 0.20$	$+0.8 \pm 0.11$	$+0.9 \pm 0.24$
	net	-2.6 ± 0.13	-0.8 ± 0.26	-3.4 ± 0.17	-3.4 ± 0.29
\bar{T}_s	(K)	-0.15 ± 0.08	$+0.01 \pm 0.05$	-0.14 ± 0.04	-0.13 ± 0.09
\bar{P}	($mm yr^{-1}$)	-7.7 ± 2.3	-0.8 ± 2.2	-8.3 ± 3.4	-8.5 ± 3.2

Note. The ERF, temperature changes, and precipitation changes are computed relative to the CONTROL Experiment. The standard deviations are computed from the annual means of years 4 to 10. ^aThe standard deviations for the sum of the two experiments are computed from the sum of the variances for the SAI and MCB-I experiments assuming independence. ^bThe LW component of the MCB-I IRF is 0 by construction.

in terms of ERF. Given the large amplification of the IRF by rapid adjustments in the SAI experiment and the relative lack of amplification in the MCB-I experiment, the ERF maxima are fairly similar in the two experiments (Figures 4b and 4d). As a consequence and given the quasi-additivity mentioned earlier, the ERF for the SAI + MCB-I experiment is fairly uniform over the globe, with the exception of Antarctica, part of the Southern Ocean, Greenland, the Sahara, and part of Australia, where the ERF is weak or positive (Figure 4f).

There is also complementarity of the IRF values in time. Time series of daily IRF for SAI and MCB-I (or MCB-DI) averaged over 10° latitude bands between 30°S and 30°N are generally anticorrelated (Figure S9). This does not hold, however, for the tropical (i.e., 30°S to 30°N) daily averages, which are positively correlated because of an interhemispheric difference in forcing which responds to seasonal variations in insolation. We cannot assess the complementarity of the ERF values in time because ERF can only be diagnosed as the difference between two simulations with different meteorologies. Hence, high-frequency variations in ERF values cannot be estimated.

4. Conclusions

We have analyzed a set of experiments aimed at diagnosing rapid adjustments in the atmosphere for the SAI and MCB solar radiation management techniques and investigating the complementarity of the two techniques. We have shown large rapid adjustments in the case of SAI with a large stratospheric warming, an increase in stratospheric humidity, and a decrease in high-level clouds. The former process appears to dominate the induced radiative effects so the ERF is much stronger than the IRF for this technique. For the first time we have combined the SAI and MCB techniques in a climate model experiment. We showed that the SAI and MCB techniques produce global mean radiative forcings that are quasi-additive. Their combination also results in a more uniform radiative forcing in space and time. It would be interesting to see if these results are corroborated by other climate models.

This study raises a number of additional questions. It would be interesting to investigate (i) if the rapid adjustments differ in a model with interactive ozone; (ii) whether the quasi-additivity holds for other aerosol types, larger radiative forcings, and/or different geographical distributions for MCB; (iii) to which extent a more uniform forcing turns into a more uniform climate response; and (iv) what impact this may have on the change in climate extremes. Fully coupled ocean-atmosphere experiments would be needed to address the last two questions. Finally, since using more than one SRM method offers more degrees of freedom, one could investigate how much scope there is and whether there is benefit from adjusting further the magnitude and spatial distribution of the different methods in order to achieve certain climate objectives (Kravitz et al., 2016).

Acknowledgments

This article is a contribution to the DFG-funded priority program SPP 1689. The authors acknowledge computing time from the TGCC under the GENCI projects t2015012201, t2016012201, and t2017012201. We thank Øivind Hodnebrog for processing the data for the calculations of the radiative effects of the rapid adjustments. The model data used in this article are available from <https://esgf.extra.cea.fr/thredds/catalog/work/oboucher/catalog.html>.

References

- Alterskjær, K., Kristjánsson, J. E., Boucher, O., Muri, H., Niemeier, U., Schmidt, H., ... Timmreck, C. (2013). Sea-salt injections into the low-latitude marine boundary layer: The transient response in three Earth System Models. *Journal of Geophysical Research: Atmospheres*, 118, 12,195–12,206. <https://doi.org/10.1002/2013JD020432>
- Boucher, O., Forster, P. M., Gruber, N., Ha-Duong, M., Lawrence, M. G., Lenton, T. M., ... Vaughan, N. E. (2014). Rethinking climate engineering categorization in the context of climate change mitigation and adaptation. *Wiley Interdisciplinary Reviews: Climate Change*, 5, 23–35. <https://doi.org/10.1002/wcc.261>
- Boucher, O., & Lohmann, U. (1995). The sulfate-CCN-cloud albedo effect: A sensitivity study using two general circulation models. *Tellus*, 47B, 281–300. <https://doi.org/10.3402/tellusb.v47i3.16048>
- Boucher, O., Randall, D., Artaxo, P., Bretherton, C., Feingold, G., Forster, P., ... Zhang, X. Y. (2013). Clouds and aerosols. In T. F. Stocker, et al. (Eds.), *Climate change 2013: The physical science basis. Contribution of working group I to the fifth assessment report of the intergovernmental panel on climate change* (pp. 571–657). Cambridge, UK: Cambridge University Press.
- Boucher, O., Schwartz, S. E., Ackerman, T. P., Anderson, T. L., Bergstrom, B., Bonnel, B., ... Yang, F. (1998). Intercomparison of models representing direct shortwave radiative forcing by sulfate aerosols. *Journal of Geophysical Research*, 103, 16,979–16,998. <https://doi.org/10.1029/98JD00997>
- Crutzen, P. J. (2006). Albedo enhancement by stratospheric sulfur injections: A contribution to resolve a policy dilemma? *Climatic Change*, 77, 211–220. <https://doi.org/10.1007/s10584-006-9101-y>
- Dessler, A. E. (2009). Clouds and water vapor in the Northern Hemisphere summertime stratosphere. *Journal of Geophysical Research*, 114, D00H09. <https://doi.org/10.1029/2009JD012075>
- Dessler, A. E., Schoeberl, M. R., Wang, T., Davis, S. M., & Rosenlof, K. H. (2013). Stratospheric water vapor feedback. *Proceedings of the National Academy of Sciences of the United States of America*, 110, 18,087–18,091. <https://doi.org/10.1073/pnas.1310344110>
- Dessler, A., Ye, H., Wang, T., Schoeberl, M., Oman, L., Douglass, A., ... Portmann, R. (2016). Transport of ice into the stratosphere and the humidification of the stratosphere over the 21st century. *Geophysical Research Letters*, 43, 2323–2329. <https://doi.org/10.1002/2016GL067991>
- Dufresne, J.-L., Foujols, M.-A., Denvil, S., Caubel, A., Marti, O., Aumont, O., ... Vuichard, N. (2013). Climate change projections using the IPSL-CM5 Earth System Model: From CMIP3 to CMIP5. *Climate Dynamics*, 40, 2123–2165. <https://doi.org/10.1007/s00382-012-1636-1>
- Environmental Pollution Panel (1965). *Restoring the Quality of Our Environment* (pp. 329). Washington, DC: White House.

- Gottelman, A., Hegglin, M. I., Son, S.-W., Kim, J., Fujiwara, M., Birner, T., ... Tian, W. (2010). Multimodel assessment of the upper troposphere and lower stratosphere: Tropics and global trends. *Journal of Geophysical Research: Atmospheres*, *115*, D00M08. <https://doi.org/10.1029/2009JD013638>
- Hourdin, F., Musat, I., Bony, S., Braconnot, P., Codron, F., Dufresne, J.-L., ... Lott, F. (2006). The LMDZ4 general circulation model: Climate performance and sensitivity to parametrized physics with emphasis on tropical convection. *Climate Dynamics*, *27*, 787–813. <https://doi.org/10.1007/s00382-006-0158-0>
- Jones, A., Haywood, J., & Boucher, O. (2011). A comparison of the climate impacts of geoengineering by stratospheric SO₂ injection and by brightening of marine stratocumulus cloud. *Atmospheric Science Letters*, *12*, 176–183. <https://doi.org/10.1002/asl.291>
- Keith, D. W. (2000). Geoengineering the climate: History and prospect. *Annual Review of Energy and the Environment*, *25*, 245–284. <https://doi.org/10.1146/annurev.energy.25.1.245>
- Kleinschmitt, C., Boucher, O., Bekki, S., Lott, F., & Platt, U. (2017). The sectional stratospheric sulfate aerosol module S3A-v1 within the LMDZ general circulation model: Description and evaluation against stratospheric aerosol observations. *Geoscientific Model Development*, *10*, 3359–3378. <https://doi.org/10.5194/gmd-10-3359-2017>
- Kravitz, B., Caldeira, K., Boucher, O., Robock, A., Rasch, P. J., Alterskjær, K., ... Yoon, J.-H. (2013). Climate model response from the geoengineering model intercomparison project (GeoMIP). *Journal of Geophysical Research: Atmospheres*, *118*, 8320–8332. <https://doi.org/10.1002/jgrd.50646>
- Kravitz, B. S., MacMartin, D., Wang, H., & Rasch, P. J. (2016). Geoengineering as a design problem. *Earth System Dynamics*, *7*, 469–497. <https://doi.org/10.5194/esd-7-469-2016>
- Kuebbeler, M., Lohmann, U., & Feichter, J. (2012). Effects of stratospheric sulfate aerosol geo-engineering on cirrus clouds. *Geophysical Research Letters*, *39*, L23803. <https://doi.org/10.1029/2012GL053797>
- Latham, J. (1990). Control of global warming? *Nature*, *347*, 339–340. <https://doi.org/10.1038/347339b0>
- Malavelle, F., Haywood, J., Jones, A., Gattelman, A., Clarisse, L., Bauduin, S., ... Thordarson, T. (2017). Evidence cloud liquid water path is invariant in aerosol-cloud interactions. *Nature*, *546*, 485–491. <https://doi.org/10.1038/nature22974>
- Myhre, G., Shine, K. P., Rädel, G., Gauss, M., Isaksen, I. S. A., Tang, Q., ... Fuglestedt, J. S. (2011). Radiative forcing due to changes in ozone and methane caused by the transport sector. *Atmospheric Environment*, *45*, 387–394.
- Niemeier, U., Schmidt, H., Alterskjær, K., & Kristjánsson, J. E. (2013). Solar irradiance reduction via climate engineering: Impact of different techniques on the energy balance and the hydrological cycle. *Journal of Geophysical Research: Atmospheres*, *118*, 11,905–11,917. <https://doi.org/10.1002/2013JD020445>
- Revell, L. E., Stenke, A., Rozanov, E., Ball, W., Lossow, S., & Peter, T. (2016). The role of methane in projections of 21st century stratospheric water vapour. *Atmospheric Chemistry and Physics*, *16*, 13,067–13,080. <https://doi.org/10.5194/acp-16-13067-2016>
- Salter, S., Sortino, G., & Latham, J. (2008). Sea-going hardware for the cloud albedo method of reversing global warming. *Philosophical Transactions of the Royal Society of London A: Mathematical, Physical and Engineering Sciences*, *366*, 3989–4006. <https://doi.org/10.1098/rsta.2008.0136>
- Schmidt, H., Alterskjær, K., Bou Karam, D., Boucher, O., Jones, A., Kristjánsson, J. E., ... Timmreck, C. (2012). Solar irradiance reduction to counteract radiative forcing from a quadrupling of CO₂: Climate responses simulated by four Earth System Models. *Earth System Dynamics*, *3*, 63–78. <https://doi.org/10.5194/esd-3-63-2012>
- Sherwood, S. C., Bony, S., Boucher, O., Bretherton, C., Forster, P. M., Gregory, J. M., & Stevens, B. (2015). Adjustments in the forcing-feedback framework for understanding climate change. *Bulletin of the American Meteorological Society*, *96*, 217–228. <https://doi.org/10.1175/BAMS-D-13-00167.1>
- Vaughan, N. E., & Lenton, T. M. (2011). A review of climate geoengineering proposals. *Climatic Change*, *109*, 745–790. <https://doi.org/10.1007/s10584-011-0027-7>